JCTC Journal of Chemical Theory and Computation

Article

pubs.acs.org/JCTC

Reference Simulations of Noncanonical Nucleic Acids with Different χ Variants of the AMBER Force Field: Quadruplex DNA, Quadruplex RNA, and Z-DNA

Miroslav Krepl,[†,#] Marie Zgarbová,[‡,#] Petr Stadlbauer,[†] Michal Otyepka,[‡] Pavel Banáš,[‡] Jaroslav Koča,[§,∥] Thomas E. Cheatham, III,[⊥] Petr Jurečka,*[,‡] and Jiří Šponer*[,†,§]

[†]Institute of Biophysics, Academy of Sciences of the Czech Republic, Kralovopolska 135, 612 65 Brno, Czech Republic

[‡]Regional Centre of Advanced Technologies and Materials, Department of Physical Chemistry, Faculty of Science, Palacky University, tr. 17 listopadu 12, 771 46, Olomouc, Czech Republic

[§]CEITEC−Central European Institute of Technology, Campus Bohunice, Kamenice 5, 625 00 Brno, Czech Republic

[∥]National Center for Biomolecular Research, Masaryk University, Campus Bohunice, Kamenice 5, 625 00 Brno, Czech Republic

[⊥]Department of Medicinal Chemistry, College of Pharmacy, University of Utah, Salt Lake City, Utah, United States

Supporting Information

ABSTRACT: Refinement of empirical force fields for nucleic acids requires their extensive testing using as wide range of systems as possible. However, finding unambiguous reference data is not easy. In this paper, we analyze four systems that we suggest should be included in standard portfolio of molecules to test nucleic acids force fields, namely, parallel and antiparallel stranded DNA guanine quadruplex stems, RNA quadruplex stem, and Z-DNA. We highlight parameters that should be monitored to assess the force field performance. The work is primarily based on 8.4 μs of 100−250 ns trajectories analyzed in detail followed by 9.6 μs of additional selected backup trajectories that were monitored to verify that the results of the initial analyses are correct. Four versions of the Cornell et al. AMBER force field are tested, including an entirely new parmχ_{OL4} variant with χ dihedral specifically reparametrized for DNA molecules containing *syn*-nucleotides. We test also different water models and ion conditions. While improvement for DNA quadruplexes is visible, the force fields still do not fully reproduce the intricate Z-DNA backbone conformation.

INTRODUCTION

The quality of explicit solvent molecular dynamics simulations of nucleic acids is primarily affected by the performance of the molecular mechanics (MM) empirical force fields.[1−4] With appropriate force fields, MD simulation techniques can provide useful insights into the structural dynamics of DNA and RNA molecules, as well as their molecular complexes.

The most widely used nucleic acid force field is the AMBER Cornell et al. parametrization.[5] Its original ff94 variant has been refined several times (ff98, ff99, parmbsc0, and parmχ_{OL3})[6−10] while some other attempts to modify it can be found in the literature.[11−13] Another fairly widely used set of nucleic acid force fields are those with CHARMM (all27, all36).[14−16]

The original variant of the Cornell et al. force field (earlier referred to as parm94 but now named ff94), when applied with explicit solvent and a proper treatment of the long-range electrostatics, provides a good description in short simulations of the B-DNA double helix and of other nucleic acids structures.[17] The main problem seemed to be an underestimation of the B-DNA double helix twisting.[18] Efforts to tune the sugar pucker and χ glycosidic torsions led to the force field variants known as ff98 and ff99.[6,7] The ff99 force field achieves a modest increase in the helical twist in B-DNA; however, in general, the performance and applicability of ff98/ff99 and ff94 are similar.

As longer simulation time scales became readily accessible, various groups reported that the force field has difficulties in reproducing experimental structures of single-stranded loops of guanine quadruplex (G-DNA) molecules.[19] Additionally, B-DNA structure progressively degrades with the ff94−99 versions due to the accumulation of γ-trans backbone substates.[8] The problem of oversampling of γ-trans has been fixed by the parmbsc0 (bsc0 in the following) variant of the force field. This was a major reparametrization of α and γ torsions enabled by high level QM studies of various phosphate sugar model systems.[8,20] The ff99+bsc0 force field modification is currently the best variant of the Cornell et al. force field to be used for the simulation of DNA.

For duplex RNA structure, all the preceding AMBER force fields are considered as having similar performance, noting that without the bsc0 modifications higher populations of γ-trans conformations are observed. In 2010, degradation of RNA molecules into senseless ladder-like structure in long simulations with all the above-noted force fields was reported and found to be due to shift of the χ torsion from the *anti* region (typical for RNA) to the high-*anti* region (typical for DNA).[21] This prompted reparametrization of the χ torsions. The parmχ_{OL} (also referred to as parmχ_{OL3}, χ_{OL3} in the

Received: April 4, 2012
Published: June 5, 2012

following) modification[9,10] prevents formation of the high-*anti* ladder-like structures, improves the shape of the *syn* region (which is important to stabilize RNA UNCG tetraloops), and improves the balance between *syn* and *anti* regions. Suppression of the high-*anti* region, however, prevents the general applicability of the χ_{OL3} force field to DNA, making χ_{OL3} an RNA-specific modification. In addition, the high-*anti* penalty, when exaggerated, reduces the inclination of A-RNA double helices. Thus, the χ_{OL3} force field finds a narrow range of *anti* to high-*anti* balance which prevents ladders while not substantially reducing the A-RNA compactness. The optimal performance of the χ_{OL3} refinement for RNA is achieved when it is combined with the bsc0 correction.[8] The AMBER suite of programs now recommends this combination of dihedral parameters for RNA simulations as part of the default set of reasonable combinations of biomolecular force fields for proteins and nucleic acids internally abbreviated as ff10.

Even with the above-described refinements, the force field is certainly far from perfect. Therefore, testing and eventual further tuning of the Cornell et al. force field variants is a major goal, since the capability of modern computers to execute long simulations is increasing steadily. In the following paper, we made two steps in this direction.

First, to enable further tuning of the force fields, it is important to have unambiguous reference experimental data. In reality, the set of available reference structures is limited. Besides canonical A-RNA and B-DNA, we can use RNA UNCG hairpin loops[9] and diagonal four-thymidine DNA quadruplex loops.[19,22] For both systems several independent but mutually consistent X-ray and NMR structures are available. Further systems are RNA GNRA tetraloops,[9] the RNA sarcin–ricin internal loop,[23,24] and perhaps a few other systems. In an attempt to identify additional reference systems, in the present study we test the available Cornell et al. force field variants for four important noncanonical nucleic acids with sufficient quality of the available X-ray structures. Namely, we study parallel-stranded and antiparallel-stranded DNA guanine quadruplex (G-DNA) stems, parallel-stranded RNA quadruplex (G-RNA) stem, and left-handed Z-DNA. Two of these systems emerged to be especially useful for testing of the force fields. Both Z-DNA and antiparallel G-DNA contain a mixture of *syn*- and *anti*-nucleotides. The antiparallel G-DNA stem shows a characteristic combination of backbone dihedral angles (see below). Z-DNA is a very specific nucleic acid form. Z-DNA is relatively rigid with a well-defined, yet unusual, alternating *syn*/*anti* χ backbone topologies and several other unusual backbone features. It is possible that the Z-DNA backbone is, compared to B-DNA, intrinsically more strained to satisfy the overall Z-DNA topology. We also test several different water models.

Second, we try to merge the advantages of the different force field variants by preparing and testing a new version of DNA Cornell et al. force field marked as parmχ_{OL4} (χ_{OL4} in the following). It aims to have improved description of the *syn* region and *syn*–*anti* balance similar to the χ_{OL3} force field while not deteriorating the B-DNA simulations due to the *anti* to high-*anti* profile. The *anti* to high-*anti* profile is in fact subtly adjusted in the opposite direction compared to the χ_{OL3} modification. It has a similar profile as the RNA χ_{OL3} force field in the *syn* region (which is a major change compared to the ff99 basic parametrization), although the *syn* region is somewhat deeper (again opposite change compared to the RNA χ_{OL3} modification) and narrower (see Methods for further details). The *syn* modification penalizes excessive population of χ *syn* angles in the region of 90–110°, as they appear to be not often populated in experimental structures.[25] The critical α/γ reparametrization has been left unchanged as in the bsc0 force field. The combined parmbsc0χ_{OL4} (abbreviated bsc0χ_{OL4}) force field shows a visible structural improvement of the antiparallel G-DNA stem. In contrast, while the force fields can achieve in general rather stable Z-DNA trajectories, none of the force fields is capable of describing all details of the Z-DNA backbone, so changes in other terms will still be needed in the future.

Although the attempted χ dihedral parameter modification is likely done in the right direction, especially for antiparallel quadruplex DNA, we would like to underline that the results need to be still taken with care. As we discussed elsewhere,[9,10] although dihedral terms have large impact on the performance of force fields in simulations, we should not expect to obtain a perfect force field by tuning the dihedral parameters. In addition, although modern QM computations can help in parametrization of the dihedral terms tremendously, the basic nature of molecular mechanics (MM) force fields remains empirical. We and others have emphasized that the ultimate judgment about the force field performance can be made only after very careful testing of the force field in extended simulations of a wide range of systems.[9,10,15] Since the number of different variants of dihedral terms that can proposed is unlimited, premature releases of modifications without extended testing may be biasing. Sometimes several dihedral profiles need to be extensively tested before recommending the optimal ones for simulations.[9,10,15] In many cases, the modified dihedral terms may fail to achieve the intended improvement of the simulation behavior or produce undesired side effects. This cannot be in advance inferred from the QM computations or from the fits of the MM terms to reproduce the QM reference data.

On the basis of the present data, we suggest that the bsc0χ_{OL4} improves structures of simulated quadruplex DNAs which represent an important class of noncanonical DNAs often studied by simulations.[26] Besides that, we demonstrate that the noncanonical NA molecules investigated in this study should be imminently included in the basic portfolio of systems that are critical for testing of new versions of the NA force fields.

METHODS

Starting Geometry and Initial Model Building. Coordinates for initial structures were taken from the X-ray structures: $d(G_4T_4G_4)_2$ G-DNA (PDB ID: 2GWQ, resolution 2.00 Å, the first molecule in the crystal lattice); $d(TGGGT)_4$ G-DNA (PDB ID: 352D, resolution 0.95 Å);[27] $r(UGGGGU)_4$ G-RNA (PDB ID: 1J8G, resolution 0.61 Å),[28] and $(CGCGCG)_2$ Z-DNA (PDB ID: 1I0T, resolution 0.6 Å).[29]

All simulations of $d(G_4T_4G_4)_2$ started with three ions in the channel and two additional ions at the stem–loop junctions, as seen in the X-ray structure. The stem–loop junction ions were, however, quickly lost, as discussed elsewhere.[22] The $d(TGGGT)_4$ structure contains unpaired thymidine residues at the ends of all strands, involved in crystal packing interactions. We removed these residues from the simulated structures to prevent structure fluctuations caused by fluctuations of these unpaired residues. The structure of $r(UGGGGU)_4$ was obtained as the biological assembly deposited in the database. We again removed the flanking uridines. Strontium cations in the channel were replaced by either sodium or potassium cations. For both parallel quadruplexes, we modified numbering

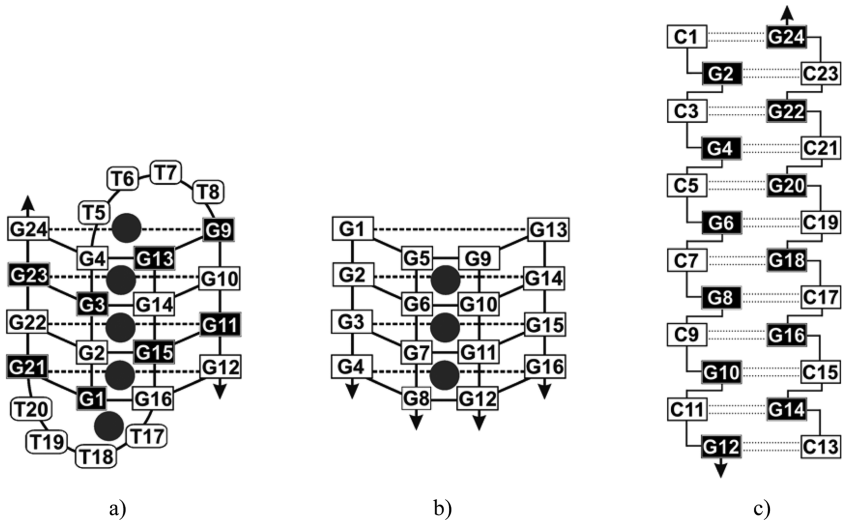

Figure 1. Scheme of the simulated structures. *Syn*-base nucleotides are marked black. Initial positions of channel ions in the quadruplex molecules are indicated. (a) $d(G_4T_4G_4)_2$ antiparallel quadruplex, (b) parallel DNA and RNA quadruplexes, and (c) Z-DNA left-handed dodecamer helix.

of the nucleotides according to the Figure 1. Structure of Z-DNA hexamer was manually lengthened to dodecamer by repeating and translating the helix to allow stable simulations. Spermine molecule was not included in the simulations.

The structures were prepared using the tLeap module of AMBER 10.[30] Systems were neutralized by adding monovalent counterions, either K^+ or Na^+ (with different parameter sets as described later). Besides simulations with net-neutralization, KCl excess salt simulations were also conducted. Added ions were distributed around the molecule by tLeap according to the solute electrostatic potential. Molecules were placed into a truncated octahedral box of explicit water solvent with a minimal distance of 10 Å of solute from the box border.

AMBER Force Fields. The AMBER simulations were carried out with the ff99,[31] bsc0,[8] χ_{OL3},[9,10] and χ_{OL4} (this work) versions of the Cornell et al. force field.[5] Bsc0 introduced significant modification to α/γ backbone torsional parameters essential for stability of B-DNA simulations. The χ_{OL3} parametrization modified the χ glycosidic torsions to stabilize RNA simulations. While χ_{OL3} modification can be combined with either ff99 or bsc0 for RNA, it works best in combination with bsc0. All DNA simulations must include bsc0.

Parmχ_{OL4} is a new version of the χ-profile that aims to improve description of the *syn* region and *syn*−*anti* balance while not deteriorating the B-DNA simulations by the *anti* to high-*anti* region. The *syn* region of χ_{OL4} profile differs from that of the RNA χ_{OL3} force field in that it provides a narrower and somewhat deeper *syn* valley than χ_{OL3}, thus suppressing the excessive population of χ *syn* angles in the region of 90°−110°. This is a result of using a deoxyribonucleoside model compound instead of the ribonucleoside one for fitting, i.e., the difference is consistent with the primary QM data. When compared to the ff99 force field, χ_{OL4} shifts the *syn* minimum to the higher χ values by about 10° and apparent are also differences in the barrier heights (Figure 2). Also, the *syn* minimum is somewhat deeper, which is an opposite trend compared to the χ_{OL3} modification. While the *syn* region was fitted to the deoxyribonucleoside QM data, the *anti* to high-*anti* region has been modified empirically. The reason is that subtle reduction of the slope of the χ correction between the *anti* and high-*anti* regions as compared to the ff99 supports the helical twist of B-DNA. It subtly increases the helical twist of B-DNA

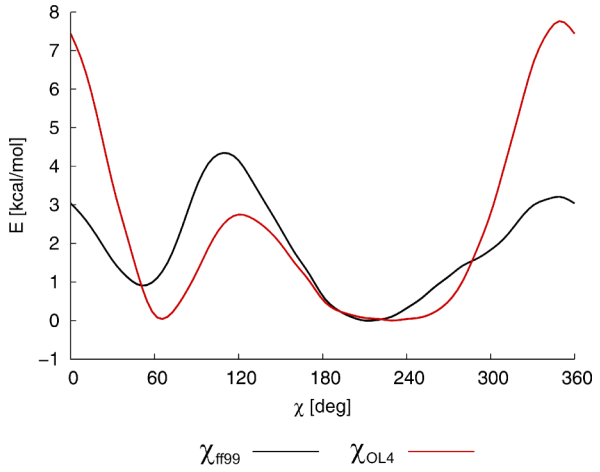

Figure 2. Gas-phase deoxyguanosine χ dihedral profile of ff99 and χ_{OL4}.

(see below) though it remains to be seen if this change can be significant for B-DNA modeling. However, the change is probably in the right direction.

Force Field Abbreviations. For the sake of brevity, we use the following abbreviations for the different modifications of the original Cornell et al. force field: ff99, bsc0, bsc0χ_{OL3}, and bsc0χ_{OL4}. These abbreviations mark the essential modifications. For the sake of completeness it should be noted that the bsc0 is fully combined with ff99. The two "OL" force fields, albeit entirely reparametrizing the χ profile, still keep the ff99 pucker parameters.

Derivation of χ_{OL4}. The χ_{OL4} parameters are based on high-quality quantum chemical profiles with inclusion of the solvation effects. The basic parametrization methodology is described elsewhere.[10] All new calculations were performed on the deoxyribonucleoside model with the 5′-OH group replaced by a hydrogen atom. Starting structures were optimized at the PBE/6-31++G(3df,3pd)[32−35] level with the continuum solvent model COSMO[36] in the TurboMole 6.2[37] software suite (water, ε_r = 78.4). QM single-point calculations were then performed at the MP2/CBS level. The complete basis set (CBS) extrapolations were obtained through the scheme of

Helgaker and Halkier[38,39] (HF and MP2 energies were extrapolated separately) using cc-pVTZ and cc-pVQZ basis sets. Turbomole 6.2 was used to calculate the MP2 energies with the RI approximation. The in-vacuo MP2/CBS energy was combined with the solvation energy taken from the PBE/LP/COSMO calculations. MM optimizations were performed with Gaussian 03[40] software suite using the "external" function and an in-house script linking Gaussian to the sander module of AMBER 9. In sander, Poisson−Boltzmann (PB) continuum solvent was used. Grid spacing was set to 0.1 Å, and default ε_r (78.4) was used. Several constraints were applied in both the MM and QM optimizations. The O4′−C4′−C3′−C2′ angle was constrained at the value 25.4° to keep the sugar pucker close to the C2′-endo conformation. The C4′−C3′−O3′−H3T angle was constrained at 180°. The O4′−C1′−N1/N9−C2/C4 (χ) angle was scanned from 0° to 360° at increments of 10° and constrained at that value. For more details about the parametrization methodology, see ref 10. The parameters of χ_{OL4} are given in the Supporting Information. A full account of the parametrization will be published separately together with in-depth analysis of the new QM data.

Preliminary B-DNA Testing. Although the main aim of this paper is to study noncanonical DNA molecules, for the sake of completeness, we carried out bsc0χ_{OL4} tests on B-DNA. Preliminary MD simulations of a canonical DNA double helix [Dickerson's dodecamer d(CGCGAATTCGCG)$_2$, 100 ns runs] with bsc0χ_{OL4} show that the force field performs well for B-DNA, with potential slight improvements of the base pair step geometries with respect to the standard bsc0 force field. For instance, for inclination the X-ray, bsc0 and bsc0χ_{OL4} values are 4.2°, 8.9°, and 8.0°, respectively, and for roll (in the same order) the values are 2.0°, 4.4°, and 4.0° (see Supporting Information, Table S1). Most importantly, the new force field increases the helical twist by almost 1°; the X-ray, bsc0, and bsc0χ_{OL4} values are 34.6°, 33.3° and 34.1°. Another improvement is found for rmsd of the backbone atoms, where the original bsc0 value of 1.95 Å was reduced to 1.74 Å with bsc0χ_{OL4} (with respect to 1BNA structure, mass weighted) and also for the major groove width, which is reduced from 19.4 Å (bsc0) to 18.4 Å with bsc0χ_{OL4}, the X-ray value being 17.3 Å. Thus, overall, the geometry of the helix is described somewhat better with our new force field, the most visible improvement being the increased helical twist. We can conclude that the new force field is suitable for B-DNA and can even bring some subtle improvement of the B-DNA architecture. We however reiterate that the change with respect to the current standard bsc0 AMBER force field in the *anti* region is quite small. The primary application area of bsc0χ_{OL4} is noncanonical DNAs. Although we think bsc0χ_{OL4} is presently the best force field for DNA systems with *syn*-nucleotides, we cannot rule out that the DNA χ profile will be further modified in the future, in case some additional parameters will be adjusted.

Cation and Solvent Conditions. Different ion and water parameters were used in the simulations. TIP3P,[41] SPC/E,[42,43] and TIP5P[44] water models were tested. We used AMBER-adapted Aqvist parameters for sodium (radius 1.8680 Å and well depth of 0.002 77 kcal/mol)[45] with TIP3P and TIP5P water models and modified Dang's parameters for potassium (radius 1.8687 Å and well depth of 0.100 kcal/mol)[46] with the SPC/E water model. We also tested the AMBER-adapted Aqvist potassium ions (radius 2.6580 Å and well depth of 0.000 328 kcal/mol).[45] However, we have seen occasional departure of these ions from the G-DNA stems. It is to be noted that this is a specific problem related to G-DNA stem simulations. The reason is excessive short-range repulsion (which may lead to ion expulsion) in simulations with K^+ inside the G-DNA stems, an effect inherent to all pair-additive force fields with r^{-12} repulsion term and described elsewhere.[22] Smith parameters (radius 2.4700 Å and well depth of 0.100 kcal/mol)[47] for chloride were used in KCl excess salt simulations in combination with Dang's K^+ parameters. Note that this selection of ion conditions is assumed to be entirely sufficient for the purpose of this paper, since the results are expected to not dramatically depend on the ion treatment. The results are assumed to be more sensitive to the water model (see below and ref 48) and primarily determined by the solute force field, which is consistent with all results given below.

Standard AMBER Molecular Dynamics Simulations. Simulations were performed with pmemd module of AMBER. The particle mesh Ewald (PME)[49,50] was used for calculation of electrostatic interactions. Covalent bonds involving hydrogen atoms were constrained using the SHAKE algorithm. Periodic boundary conditions, a 2 fs integration step and 300 K temperature (Berendsen weak-coupling)[51] were used. We used standard equilibration and production inputs.[52,53] Analyses of resulting trajectories were performed using ptraj module of AMBER, and the VMD program[54] was used for visualization.

Analyses. To make our presentation compact, the dihedral angle, sugar pucker,[55] and rmsd analyses presented in the paper are primarily based on median values from simulation trajectory ends. We used a 50−100 ns interval for quadruplex molecules. An interval of 85−100 ns (220−250 ns for 250 ns long simulations) was used for Z-DNA molecule. For graphs and additional data, see the Supporting Information. Nevertheless, all simulations were monitored on entire simulation time scales to guarantee that we do not miss any significant development. Likewise, the individual torsions were monitored to guarantee that the results directly shown in the paper are in all aspects representative. Time intervals used for presented analyses were found to be fully representative of the simulation developments.

Performance of force fields for quadruplex molecules was evaluated primarily by comparing simulation results with the experimental values from the starting structures. For Z-DNA, comparison with reference values of Z-DNA backbone torsions[25] was used instead. The reason is that the individual structures of Z-DNA molecules in the database show irregularities in the individual backbone angle distributions. Thus, in this particular case we rather rely on nucleic acids backbone families as derived by structural bioinformatics. Terminal residues were not considered in this comparison, as they do not follow rules typical for Z-DNA molecules.

The force fields are often assessed on the basis of deviations of the dihedrals in simulations from the reference values, calculated as the simulation value minus the reference value.

Results for TIP5P water model were somewhat different from the rest of the simulations and are discussed separately.

RESULTS

Simulations of the d(G$_4$T$_4$G$_4$)$_2$ Antiparallel Quadruplex. The antiparallel quadruplex consists of two d(G$_4$T$_4$G$_4$) strands that form four guanine tetrads and two four-thymidine diagonal loops. Three potassium ions are located between tetrads in the G-stem. One potassium ion is located at each stem−loop junction.[56] In Na^+ simulations, the original potassium ions in G-stem and loop regions were replaced with sodium. Earlier studies demonstrated that neither the

stem−loop ion binding nor the four-thymidine loops are correctly described by contemporary simulations,[22] which is confirmed also by the present simulations (data not shown, see ref 22). Thus, we concentrate our analyses on the four-tetrad stem of this G-DNA molecule, with its alternating *syn*−*anti*-nucleotide conformations.

Table 1 summarizes the $d(G_4T_4G_4)$ simulations. Tables 2 and 3 summarize the range of the backbone angles seen in the experimental structure for all 16 nucleotides in the stem. Other X-ray structures of the same molecule available in the database show very similar results. The individual nucleotides have variable backbone angles, which may partially be real structural differences and partially resolution limits/packing effects of the X-ray structure. (Note that by packing effects we mean not only evident atomic contacts but also any subtle differences of the environment, which may modestly influence the backbone dihedrals). Thus, it is not possible to determine "exact" target values of the dihedrals. Nevertheless, evaluation of all 16 stem nucleotides reveals some clear trends, especially for combination of the essential α/γ backbone substates (Table 3) and sugar puckers. Since the inner tetrads are better defined in the experiment and they are shielded from the end effects, we suggest that the inner tetrads provide the best benchmark for force field testing.

Table 1. List of Simulations of the $d(G_4T_4G_4)_2$ Antiparallel Quadruplex

simulation name	ion type and condition[a]	solvent type	trajectory length, ns
Simulations with ff99			
antipardna_1_99	Na^+	TIP3P	200
Simulations with bsc0			
antipardna_1_bsc0	Na^+	TIP3P	200
antipardna_2_bsc0	Na^+	TIP5P	100
antipardna_3_bsc0	K^+	SPC/E	200
antipardna_4_bsc0	KCl	SPC/E	200
fixSPCE_from_bsc0[b]	K^+	SPC/E	200
Simulations with bsc0χ_{OL3}			
antipardna_1_OL3	Na^+	TIP3P	200
antipardna_2_OL3	Na^+	TIP5P	100
antipardna_3_OL3	K^+	SPC/E	200
antipardna_4_OL3	KCl	SPC/E	200
Simulations with bsc0χ_{OL4}			
antipardna_1_OL4	Na^+	TIP3P	200
antipardna_2_OL4	Na^+	TIP5P	200
antipardna_3_OL4	K^+	SPC/E	200
antipardna_4_OL4	KCl	SPC/E	200
fixOL4_from_bsc0[b]	Na^+	TIP3P	100

[a]Cation concentration was approximately 0.35 M for minimum-salt (i.e., net-neutral) conditions. Additional 0.2 M of KCl were used for excess-salt simulations. [b]Simulation starting with the final structure of antipardna_1_bsc0 simulation, where the backbone adopts already different substates compared to the start.

Table 2. Dihedral Angles (in deg) and Pucker of Antiparallel Quadruplex in the Starting 2GWQ (the first molecule) X-ray Structure

	outer tetrads		inner tetrads	
dihedral	*syn*-nucleotides (G1, G9, G13, G21)	*anti*-nucleotides (G4, G12, G16, G24)	*syn*-nucleotides (G3, G11, G15, G23)	*anti*-nucleotides (G2, G10, G14, G22)
β	210 ± 18	180 ± 12	204 ± 43	175 ± 8
δ	139 ± 3	134 ± 4	143 ± 7	132 ± 3
ε	177 ± 3	164 ± 4	184 ± 10	185 ± 6
ζ	281 ± 8	285 ± 3	278 ± 8	246 ± 31
χ	60 ± 6	259 ± 9	61 ± 6	244 ± 10
P	160 ± 6	148 ± 6	165 ± 14	143 ± 4

Table 3. α/γ Dihedral Combinations of Antiparallel Quadruplex in the Starting X-ray Structure[a]

α/γ combinations	nucleotides	mean values
$\alpha(-)/\gamma(+)$	G2, G4, G10, G12, G14, G16, G22, G24	292/53
$\alpha(+)/\gamma(-)$	G3, G15, G23	50/296
$\alpha(+)/\gamma(t)$	G9, G21	71/200
$\alpha(-)/\gamma(-)$	G11	302/311

[a]The first nucleotides in each strand, G1 and G13, possess $\gamma(+)$ angles.

The stem is basically stable in all simulations; however, there are visible differences among the force fields in description of the backbone angles. The RNA-specific bsc0χ_{OL3} parameters initially appear to improve description of G-stem dihedrals and pucker (especially for the *syn*-guanine nucleotides) compared to ff99 and bsc0 simulations. However, this improvement is eventually obliterated on longer time scales, and in the end, performance of bsc0χ_{OL3} is comparable with ff99 and bsc0 (see Methods for the force field abbreviation).

The bsc0χ_{OL4} variant improves G-stem dihedrals and puckers on the entire simulation time scales. It keeps better the starting experimental values of backbone dihedrals and clearly tends to restore them when starting a simulation from structure previously perturbed by another force field (Figure 3, bottom). In other words, the "*syn*-refined" bsc0χ_{OL4} force field visibly structurally improved simulations of antiparallel G-DNA stems. The results are summarized in Tables 4−7 and more extensively documented in the Supporting Information (Tables S2−S6 and Figures S1−S4). The improvement is best visible for the pucker, χ and δ angles, where the bsc0χ_{OL4} force field is the only variant that is consistently in agreement with experiment for the residues of the inner tetrads (see Tables 4 and 6).

Intricate Pucker and α/γ and β Correlation in Antiparallel G-DNA Stem. In the initial (experimental) structure, all *anti*-base nucleotides have canonical $\alpha(-)/\gamma(+)$ dihedrals while *syn*-base nucleotides have three distinct noncanonical α/γ dihedral combinations. The outer tetrads (G9 and G21, note the 5′-end G1 and G13 lack phosphates) show $\alpha(+)/\gamma(t)$ combination. The inner tetrads (G3, G11, G15, and G23) are either $\alpha(+)/\gamma(-)$ or $\alpha(-)/\gamma(-)$. Additionally, $\alpha(-)/\gamma(-)$ is always coupled with an unusual β dihedral (~260°). We observed such distribution also in X-ray structures of other antiparallel quadruplexes, which suggests that it is a general experimental rule for their backbone configuration (for example, see PDBs 1JB7,[57] 2AVH,[58] 3NZ7,[59] and 2HBN[60]).

The α/γ dihedrals of stem *anti*-nucleotides are reasonably well maintained in all simulations. Surprisingly, we have not observed accumulation of γ-trans dihedrals in ff99 simulation without the bsc0 correction, sharply contrasting ff99 B-DNA simulations. The $\gamma(t)$ flips are present, but reversible. This is confirmed by 1 μs control simulation (see below) and illustrates the delicacy of the force fields and their application to different nucleic acids forms. Likewise, the α/γ dihedrals of

Figure 3. α/γ dihedral development for *syn*-nucleotides (G9 and G21 belong to the outer tetrads) of the antiparallel quadruplex, Na^+,TIP3P simulations. Top, bsc0 simulation; middle, bsc0χ_{OL4} simulation; bottom, bsc0χ_{OL4} simulation starting from the bsc0 simulation end (cf. Table 1). Bsc0 irreversibly assumes incorrect dihedrals early in the simulation. Bsc0χ_{OL4} shows only short-living flips of the α/γ dihedrals (and pucker—see the text) into incorrect values and also restores the correct values when structure with incorrect values is taken as the start.

outer *syn*-base nucleotides (G9 and G21) are well maintained in all simulations (Figures 3 and 4).

The X-ray structures and simulations reveal tight coupling between the α/γ dihedrals, β dihedral, and sugar pucker in the inner *syn*-base nucleotides. Both in X-ray structure and in simulations, high C2′-endo region (160°−185°) is coupled with $\alpha(-)/\gamma(-)$ and $\beta(\sim 260°)$, while low C2′-endo region (135°−

Table 5. Populations (in %) of Different α/γ *syn*-Nucleotide Combinations of Antiparallel G-DNA Stem in Na^+-net neutral simulations in TIP3P (the 50−100 ns period)[a]

	nucleotides	$\alpha(-)/\gamma(+)$	$\alpha(+)/\gamma(-)$	$\alpha(+)/\gamma$(t)	$\alpha(-)/\gamma(-)$
x-ray		–	G3, G15, G23	G9, G21	G11
ff99	G3	92	3	0	0
	G9	0	0	100	0
	G11	97	0	0	1
	G15	93	1	0	5
	G21	0	0	100	0
	G23	84	4	0	7
bsc0	G3	100	0	0	0
	G9	41	0	59	0
	G11	100	0	0	0
	G15	100	0	0	0
	G21	1	0	99	0
	G23	100	0	0	0
bsc0χ_{OL3}	G3	100	0	0	0
	G9	18	0	82	0
	G11	52	17	0	30
	G15	69	25	0	6
	G21	14	0	86	0
	G23	36	35	0	29
bsc0χ_{OL4}	G3	34	41	0	25
	G9	0	0	100	0
	G11	36	36	0	27
	G15	55	27	0	19
	G21	49	0	51	0
	G23	21	55	0	24

[a]The canonical $\alpha(-)/\gamma(+)$ combination is not in agreement with the experiment. G9 and G21 should be $\alpha(+)/\gamma$(t) and the remaining nucleotides are compatible with both $\alpha(+)/\gamma(-)$ and $\alpha(-)/\gamma(-)$.

Table 4. Deviations of Dihedral Angles and Pucker (in deg) of Antiparallel G-DNA Stem from the Reference Structure;[a] Na^+-Net Neutral Simulation in TIP3P[b]

	outer tetrads									
	syn-nucleotides (G1, G9, G13, G21)					*anti*-nucleotides (G4, G12, G16, G24)				
dihedral	X-ray	ff99	bsc0	bsc0χ_{OL3}	bsc0χ_{OL4}	X-ray	ff99	bsc0	bsc0χ_{OL3}	bsc0χ_{OL4}
β	210	−24	−25	−10	−26	180	−6	−7	−9	−10
δ	139	+2	−6	+2	±0	134	+3	+3	−1	+1
ε	177	+8	+7	+4	+3	164	+17	+16	+17	+15
ζ	281	−4	−4	−6	−6	285	−12	−12	−11	−12
χ	60	−2	−3	+3	+4	259	−4	−4	−7	−2
P	160	−3	−16	−4	−5	148	+3	+3	−4	−2
	inner tetrads									
	syn-nucleotides (G3, 11, 15, 23)					*anti*-nucleotides (G2, 10, 14, 22)				
dihedral	X-ray	ff99	bsc0	bsc0χ_{OL3}	bsc0χ_{OL4}	X-ray	ff99	bsc0	bsc0χ_{OL3}	bsc0χ_{OL4}
β	204	−28	−30	−23	−20	175	−8	−8	−9	−7
δ	143	−44	−46	−24	−5	132	−24	−29	−19	−5
ε	184	+10	+10	+5	+5	185	±0	±0	+4	+4
ζ	279	±0	−1	−3	−3	246	+21	+24	+23	+7
χ	61	−18	−18	−6	−3	244	−10	−13	−11	−2
P	165	−61	−65	−34	−8	143	−28	−37	−24	−6

[a]MD − X-ray, for the 50-100 ns period. Median simulation values are used; see Methods. [b]The average X-ray values are given as the first item on each line. See Figure S1 (Supporting Information) for the values obtained for the individual nucleotides.

Table 6. Deviations of Dihedral Angles and Pucker (in deg) of Antiparallel G-DNA Stem from the Reference Structure;[a] K^+-Net Neutral Simulation in SPC/E[b]

	outer tetrads							
	syn-nucleotides (G1, G9, G13, G21)				*anti*-nucleotides (G4, G12, G16, G24)			
dihedral	X-ray	bsc0	bsc0χ_{OL3}	bsc0χ_{OL4}	X-ray	bsc0	bsc0χ_{OL3}	bsc0χ_{OL4}
β	210	−9	−23	−12	180	−10	−10	−10
δ	139	+1	+2	+4	134	+2	−1	+2
ε	177	+6	+3	+3	164	+16	+16	+15
ζ	281	−4	−6	−6	285	−4	−11	−13
χ	60	−2	+4	+5	259	±0	−5	+1
P	160	−8	−3	−1	148	−11	−5	−1
	inner tetrads							
	syn-nucleotides (G3, G11, G15, G23)				*anti*-nucleotides (G2, G10, G14, G22)			
dihedral	X-ray	bsc0	bsc0χ_{OL3}	bsc0χ_{OL4}	X-ray	bsc0	bsc0χ_{OL3}	bsc0χ_{OL4}
β	204	−22	−24	+2	175	−8	−9	−7
δ	143	−19	−4	+6	132	−6	−6	+1
ε	184	+5	+5	+4	185	+4	+5	+7
ζ	279	±0	−2	−1	246	+16	−11	±0
χ	61	−11	−6	−1	244	−2	−7	+1
P	165	−31	−9	+7	143	−7	−9	±0

[a]MD − X-ray, the 50-100 ns period. [b]The average X-ray values is the first item on each line. See Figure S3 (Supporting Information) for the values obtained for the individual nucleotides.

Table 7. Populations of Different α/γ *syn*-Nucleotide Combinations of Antiparallel G-DNA Stem in K^+-Net Neutral Simulations in SPC/E (the 50−100 ns period)[a]

	nucleotides	$\alpha(-)/\gamma(+)$	$\alpha(+)/\gamma(-)$	$\alpha(+)/\gamma$(t)	$\alpha(-)/\gamma(-)$
x-ray		–	G3, G15, G23	G9, G21	G11
bsc0	G3	65	32	0	3
	G9	0	0	100	0
	G11	36	29	0	36
	G15	51	25	0	11
	G21	0	0	100	0
	G23	48	25	0	27
bsc0χ_{OL3}	G3	60	40	0	0
	G9	0	0	100	0
	G11	9	74	0	18
	G15	24	75	0	1
	G21	0	0	100	0
	G23	8	90	0	2
bsc0χ_{OL4}	G3	4	78	0	19
	G9	0	0	100	0
	G11	8	17	0	75
	G15	16	80	0	5
	G21	0	0	100	0
	G23	14	42	0	44

[a]The canonical $\alpha(-)/\gamma(+)$ combination is not in agreement with the experiment. G9 and G21 should be $\alpha(+)/\gamma$(t) and the remaining nucleotides are compatible with both $\alpha(+)/\gamma(-)$ and $\alpha(-)/\gamma(-)$.

160°) is coupled with $\alpha(+)/\gamma(-)$ and β essentially in trans. Repuckering to O4′-endo/C1′-exo in simulations (not seen in experiment) is tightly coupled with changes in α/γ dihedrals to the canonical $\alpha(-)/\gamma(+)$ combination, as illustrated in Figure 5. Correct force field description of the sugar pucker is thus essential for correct description of α/γ dihedrals and vice versa. Development of α/γ dihedrals is also an excellent indicator of sugar pucker development (Figure 5), i.e., repuckering and α/γ flips are perfectly correlated. On the basis of the currently

Figure 4. α/γ dihedral development for *syn*-nucleotides (G9 and G21 belong to the outer tetrads) of the antiparallel quadruplex, K^+, SPC/E simulations. Top, bsc0 simulation; middle, bsc0 simulation starting from antipardna_1_bsc0 TIP3P simulation (cf. Table 1); bottom, bsc0χ_{OL4} simulation. Bsc0 produces a larger population of incorrect (canonical) values than bsc0χ_{OL4}. Bsc0 alone also does not completely restore the structure when the previously perturbed structure is taken as the start. Nucleotides G11 and G23 were mostly restored while G3 and G15 retained predominantly incorrect values. Note that positions of G11/G23 and G3/G15 nucleotides in the quadruplex are not completely equivalent, which may cause their somewhat different behavior in simulations (Figure 1).

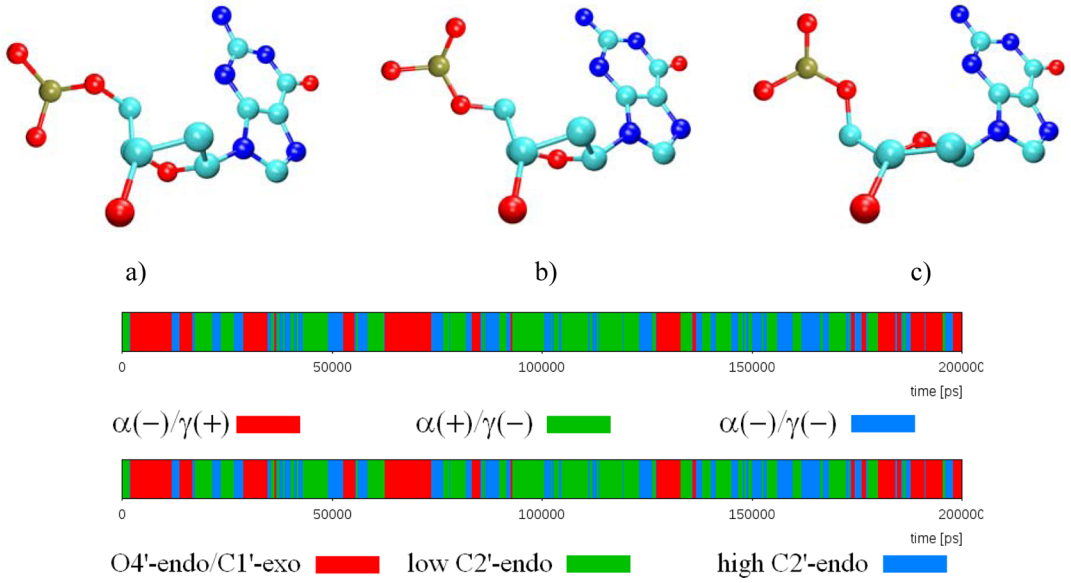

Figure 5. Coupling of sugar pucker and associated α/γ combinations for *syn*-nucleotides in inner tetrads. (a) High C2′-endo, $\alpha(-)/\gamma(-)$; (b) low C2′-endo, $\alpha(+)/\gamma(-)$; (c) O4′-endo/C1′-exo, $\alpha(-)/\gamma(+)$. The example is from simulation development of nucleotide G3 in simulation antipardna_1_OL4. Both regions of C2′-endo pucker are populated in the experiment. The O4′-endo/C1′-exo pucker is sampled in simulations but it is not seen in experiments. It is only a minor substate with the bsc0χ_{OL4}.

available data, we consider the $\alpha(+)/\gamma(-)$ and $\alpha(-)/\gamma(-)$ substates of the inner-tetrad *syn*-nucleotides as equally compatible with the G-DNA structure, so we assume they can alternate.

Bsc0χ_{OL4} is the only force field that stays in reasonable agreement with experiments for the inner-tetrad *syn*-nucleotides. Albeit fluctuations to canonical α/γ values and O4′-endo/C1′-exo do occur, they are always reversible (Figure 3, middle). The other force fields (see below for water model differences) tend to permanently change the inner *syn*-nucleotides to canonical α/γ values and thus "lock" the backbone in an incorrect conformation (Figure 3, top). An accurate description of sugar-pucker by the available force fields, including the coupling between sugar pucker and the other parameters (namely χ), is a well-known problem.[10] Thus, an important observation is that, with the exception of bsc0χ_{OL4}, all other tested force fields tend to incorrectly describe sugar pucker and α/γ in the antiparallel G-DNA stem inner tetrads, which sooner or later irreversibly change from the experimental C2′-endo region to the O4′-endo/C1′-exo region (∼100°) with concomitant α/γ flips.

The simulations also reveal some effect of the environment. We observed a difference between TIP3P and SPC/E water models. With TIP3P, all force fields (except bsc0χ_{OL4}) shift the pucker of inner *syn*-nucleotides permanently (Figure 3). With SPC/E, this rearrangement is slower and may be partially reversible on the present simulation time scale even with the other force fields (Figure 4, top). However, even with SPC/E, bsc0χ_{OL4} still gives better results than bsc0 as the pucker distribution is more in favor of the experimental region (Figure 4, bottom). Further, when not using χ_{OL4} and starting from a structure with an incorrect backbone topology (Figure 4, middle), the simulations in SPC/E do not repair the backbone angles. In the example shown in the middle of Figure 4, backbone conformations of nucleotides G11 and G23 are mostly restored while nucleotides G3 and G15 remain predominantly in the incorrect pucker. These results support our earlier observation (together with unpublished data for some other systems) that there is certain coupling between the solute force field performance and the water model.[48] Although the TIP3P and SPC/E simulations were carried out with different ion conditions, on the basis of our recent RNA simulation studies and some additional unpublished data we suggest that the observed differences are mainly attributable to the water model.[48]

In summary, the bsc0χ_{OL4} is the only tested force field that does not irreversibly convert (under any tested conditions) the sugar pucker of the inner tetrads to the O4′-endo/C1′-exo region. If visiting this state it is only a temporary event. Accordingly, it keeps the correct α/γ substate. Further, as noted above, it reverses the O4′-endo/C1′-exo states back to C2′-endo when simulated structures obtained by the other force fields are taken as the start (Figure 3, bottom).

It should be noted that the Tables 2−7 take the first molecule of the 2GQW X-ray structure as the reference. The remaining three crystallographically independent molecules of the 2GQW structure have obviously somewhat different individual backbone torsion values, and the same is also true for the 1JPQ structure of the same molecule. In some cases, the equivalent nucleotides may adopt different substates, when two substates can compete, for example, in case of the $\alpha(-)/\gamma(-)$ and $\alpha(+)/\gamma(-)$ substates of the inner-tetrad *syn*-nucleotides. Nevertheless, the choice of the reference geometry has no effect on any conclusion of our work. Our main judgment regarding better performance of bsc0χ_{OL4} vs bsc0 remains entirely unaffected. This is documented in the Supporting Information, where Table S7 lists the backbone dihedrals in all five independent experimental structures mentioned above while Tables S8 and S9 show a re-evaluation of the key Table 4 for the inner tetrads by considering the other structures as reference data.

Simulations of the d(G$_4$)$_4$ Parallel Quadruplex. The parallel quadruplex consists of four dG$_4$ chains that form four *all-anti*-guanine tetrads. Three sodium ions are located between

Table 8. Deviations of Dihedral Angles and Pucker (in deg) of Parallel G-DNA Stem from the Reference Structure;[a] Na^+-Net Neutral Simulation in TIP3P[b]

	outer tetrads[c] (G1, G4, G5, G8, G9, G12, G13, G16)					inner tetrads (G2, G3, G6, G7, G10, G11, G14, G15)				
dihedral	X-ray	ff99[d]	bsc0	bsc0χ_{OL3}	bsc0χ_{OL4}	X-ray	ff99[e]	bsc0	bsc0χ_{OL3}	bsc0χ_{OL4}
α	292	−3 (−3)	−5	−4	−6	289	−3 (−47)	−1	±0	−1
β	181	−4 (−4)	−5	−6	−4	193	−15 (−27)	−19	−19	−17
γ	48	+2 (+2)	+6	+7	+5	47	+8 (+56)	+10	+11	+10
δ	139	−8 (−7)	−16	−26	−12	134	−17 (−15)	−21	−25	−15
ε	176	N/A (+56)	+18	+21	+17	187	+2 (+4)	+1	+1	+1
ζ	263	N/A (−66)	+13	+19	+13	255	+15 (+17)	+15	+16	+13
χ	243	+1 (+13)	−14	−25	−9	250	−20 (−27)	−23	−25	−19
P	156	−15 (−14)	−24	−39	−18	153	−27 (−24)	−34	−40	−25

[a](MD − X-ray, the 50-100 ns period median values; see Methods). [b]The average X-ray values is the first item on each line. [c]Dihedrals α, β, and γ of 5′-end terminal nucleotides (G1, G5, G9, G13) and dihedrals ε and ζ of 3′-end terminal nucleotides (G4, G8, G12, G16) are not considered. [d]Nucleotides G1, G5, G9, G13 are not considered since they are heavily affected by irreversible $\alpha(+)/\gamma(t)$ and $\beta(+)/\gamma(t)$ flips; that is also why no values of ε and ζ are given. Values in parentheses show average median if no nucleotides are omitted. [e]Nucleotides G2, G6, G10, G14 are not considered since they are substantially affected by irreversible $\alpha(+)/\gamma(t)$ and $\beta(+)/\gamma(t)$ flips. Values in parentheses show the average median if no nucleotides are omitted.

Table 9. Populations of the Main Flipped Substates in the Interval (50−100 ns) of Each Parallel G-DNA Simulation[a]

	ff99		bsc0		bsc0χ_{OL3}		bsc0χ_{OL4}	
	$\alpha(+)/\gamma(t)$	$\beta(+)/\gamma(t)$	$\alpha(+)/\gamma(t)$	$\beta(+)/\gamma(t)$	$\alpha(+)/\gamma(t)$	$\beta(+)/\gamma(t)$	$\alpha(+)/\gamma(t)$	$\beta(+)/\gamma(t)$
Na^+ TIP3P	13.0	11.6	0.2	2.3	0	0	1.8	2.3
K^+ SPC/E	N/A		2.2	1.6	0	0	0.7	0.1
KCl SPC/E	N/A		0.6	8.6	1.2	2.1	0.4	1.9

[a]The numbers show the percentage of flipped population in all nucleotides during the whole interval. Ff99 simulation is already visibly affected by the flips which accumulate with ff99.

the tetrads. In K^+ simulations, the sodium ions were replaced with potassium ions. In the Supporting Information Table S10 summarizes the simulations while Table S11 presents average values of torsion angles in the experimental structure.

The stem remained visually stable during all simulations. The bsc0 and bsc0χ_{OL4} force fields performed best. We observed several very short and reversible α/γ and β/γ flips, which are described below. The frequency of α/γ and β/γ transitions was generally higher in the SPC/E water model compared to TIP3P with both force fields. Further, with TIP3P, the frequency was higher in bsc0χ_{OL4} simulations, while with SPC/E it was higher when using bsc0. This, however, may still be influenced by the simulation length. The simulations with the SPC/E water model showed increased pucker in comparison with TIP3P. The results of bsc0 and bsc0χ_{OL4} seem comparable for backbone angles, but the χ_{OL4} modification brings a visible improvement in pucker and χ description (Table 8 and Supporting Information, Tables S12−S13). As noted above, we have subtly modified the *anti* to high-*anti* χ profile compared to the preceding force fields, which appears to be profitable for this particular system. Note that values of δ, χ, and pseudorotation P, especially for the inner tetrads, are still somewhat different from the 0.95 Å X-ray structure (Table 8 and Supporting Information, Tables S12−S13). Thus, even with the bsc0χ_{OL4} description the computed χ values in inner tetrads differ by 19° (13° in SPC/E) from the target experimental values. Therefore, while the general performance of the force fields for the parallel G-DNA stem is very good, further refinement of the force field might still improve the detailed description of the structure.

The RNA-specific bsc0χ_{OL3} lowered χ, δ, and significantly pucker of both inner and outer tetrads (Table 8 and Supporting Information , Tables S12 and S13).

When simulated with ff99, the structure looked at first sight quite correct during the whole simulation, but detailed analysis showed problems with irreversible α/γ and β/γ flips similar to B-DNA ff99 simulations.[8] The first transition occurred after 35 ns in the second tetrad and was followed by several others. The G-stem was already significantly affected by the force field at the end of our simulation without the bsc0 correction. We identified several noncanonical substates of the G-stem during the simulation. Strongly underestimated helical twist was a typical problem observed in all these substates (see Supporting Information , Figure S5). However, previous studies with ff99 without the bsc0 correction were probably not dramatically affected, because their time scales were too short to develop large problems; further, the effect does not seem to be as detrimental as observed for B-DNA.[8] The ff99 simulation behavior before occurrence of the backbone flips is similar to bsc0 simulation.

Detailed Description of $\beta(+)/\gamma(t)$ Flip in Simulations of Parallel G-DNA Stem. As noted above, we observed β/γ substates mainly described by values of dihedral angles $\beta(+)$ and $\gamma(t)$. The flip had preference to occur in nucleotides of the second tetrad, which is probably caused by larger fluctuations of the first tetrad. The flips occurred in all force fields to a certain extent, being a major irreversible issue with parm99 while being reversible when bsc0 and bsc0χ_{OL4} were applied (see Table 9). This substate was almost always preceded and followed (if reversed) by $\alpha(+)/\gamma(t)$ flip common in B-DNA ff99 simulations.[8] Duration of the $\alpha(+)/\gamma(t)$ intermediate substate varied from tens of picoseconds to tens of nanoseconds. The $\alpha(+)/\beta(t) \rightarrow \alpha(-)/\beta(+)$ flip occurred between the $\alpha(+)/\gamma(t)$ and $\beta(+)/\gamma(t)$ substates (Figure 6). Direct $\beta(t)/\gamma(+) \rightarrow \beta(+)/\gamma(t)$ flips were found in some cases. We also revealed other more complex mechanisms consisting of up to nine flips, but

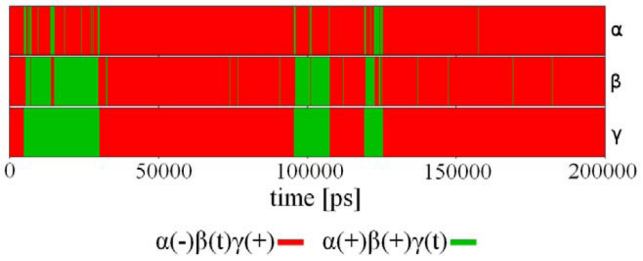

Figure 6. Development of α, β, and γ dihedral angle values of nucleotide G14 in net-neutral Na^+, TIP3P simulation of parallel G-DNA with bsc0χ_{OL4} force field during a typical formation, interruption, and termination of the $\beta(+)/\gamma(t)$ substate in cooperation with the intermediate $\alpha(+)/\gamma(t)$ substate.

these were rare. The $\beta(+)/\gamma(t)$ substate led to increased pucker fluctuation and decreased χ value of the affected nucleotide and decreased pucker fluctuation and increased χ value of the preceding nucleotide (Table 10).

Simulations of the r(G$_4$)$_4$ Parallel Quadruplex. The parallel quadruplex consists of four rG$_4$ chains with all-*anti* orientation. The Supporting Information (Table S14) shows average experimental values of torsion angles. The ultrahigh resolution structure appears to be substantially affected by crystal packing. There are only four crystallographically independent nucleotides (one strand) while there are numerous tight crystal packing contacts. The crystallization conditions resulted in Sr^{2+} in the channel, which is difficult to describe correctly by pair-additive force fields. The experimental structure contains, in our opinion, profound irregularities.

The stem remained stable during all simulations. Increased fluctuations of nucleotides in the first tetrad were observed. The results are summarized in the Supporting Information (Tables S15−S20). We suggest that the RNA-specific bsc0χ_{OL3} is the best performing force field. It drove outlying dihedral angle values found in the initial structure to canonical values in 5 ns and retained canonical values of dihedrals for the whole length of simulations. Almost no α/γ and β/γ transitions were observed and pucker was described correctly with very few and very short visits to the C2′-endo region. More importantly, the other force fields promoted occasional shifts of χ to the high-*anti* χ. Although it occurred only few times for individual nucleotides on the present time scale, it indicates that longer simulations without χ_{OL3} may ultimately accumulate such flips, leading to a ladder-like structure.[9,10,21,48] Ff99 simulation, in addition, was affected by α/γ flips (see Supporting Information, Tables S18−S20). The DNA-specific bsc0χ_{OL4} incorrectly described δ, χ, and pucker, as expected (see Supporting Information for detailed analysis). In summary, the all-parallel G-RNA quadruplex may be used as reference structure to test force fields; however, we strongly advise one to use its idealized structure with canonical backbone instead of the X-ray geometry. Bsc0χ_{OL3} is presently the best variant.

Simulations of the Z-DNA Dodecamer. The simulated Z-DNA helix consists of two antiparallel strands with d(CG)$_6$ sequence. Dihedral angles in Z-DNA are quite distinct from other DNA molecules. Table S21 (Supporting Information) summarizes the simulations that have been carried out while Table 11 summarizes the typical experimental Z-DNA backbone conformation families.[25] All guanine nucleotides have *syn*-base configuration and their α/γ dihedrals are always $\alpha(+)/\gamma(t)$. While the 5′-CpG-3′ dinucleotide step has only one possible conformation (Z-form), two forms (ZI-form and ZII-form) are possible for the 5′-GpC-3′ dinucleotide step.[25] This is because the repeating unit of Z-DNA is the dinucleotide. Guanine and cytosine nucleotides then can have different reference dihedrals (Table 11). There is the following well-established "ZI/ZII" rule of the GpC dinucleotide repeating unit. When a given (N) guanine has ζ around 290°, the subsequent (N + 1) cytosine must have β around 235°. When a given guanine has ζ around 65°, the subsequent (N + 1) cytosine must have β around 160°.

Table 11. Reference Values of Dihedral Angles (deg) in Z-DNA[25]

	Z-form			
	cytosine nucleotides		guanine nucleotides	
dihedral	ZI-form[a]	ZII-form[a]	ZI-form[a]	ZII-form[a]
α	210	169	66	
β	233	162	186	
γ	54	44	179	
δ	144		95	
ε	264		242	187
ζ	76		292	63
χ	205		61	
P^b	155		30−90	

[a]Different values for the ZI and ZII forms (5′-GpC-3′ dinucleotide step) are given where relevant. [b]Pucker of guanine nucleotides is given as a possible range rather than a single value.

For guanine nucleotides, experimental sugar pucker is in a pseudorotation range of 30−90° (C3′-endo to O4′-endo). Guanine nucleotides at the beginning or end of strands have C2′-endo pucker. They also have dihedrals that are not typical for the rest of the Z-DNA molecule and we do not consider them in the tables. Sugar puckers of cytosine nucleotides fall into the C2′-endo range. Since sugar pucker is not analyzed in detail in ref 25, we estimated it from the experimental structure. Our estimated pucker values are in accordance with the text description in ref 25 and with values of the associated δ dihedrals of the respective nucleotides (Table 11). We also observed similar values in other experimental structures of Z-DNA (PDB IDs: 3P4J, [61] 1ICK, [62] 1DCG, [63] etc.).

ZI and ZII Conformers Are Not Fully Accurately Described by Available Force Fields. We suggest that although the simulations provide rather stable ∼250 ns scale

Table 10. Medians of Backbone Angles of Canonical $\beta(t)/\gamma(+)$ State and $\beta(+)/\gamma(t)$ Substate in SPC/E, KCl Simulation of d(GGGG)$_4$[a]

	$\delta(n-1)$	$P(n-1)$	$\chi(n-1)$	$\varepsilon(n-1)$	$\zeta(n-1)$	$\alpha(n)$	$\beta(n)$	$\gamma(n)$	$\delta(n)$	$P(n)$	$\chi(n)$	$\varepsilon(n)$	$\zeta(n)$	$\alpha(n+1)$
canonical substate	129	141	237	191	273	288	177	55	129	143	239	189	264	288
flipped substate	130	138	273	195	276	265	65	176	119	133	193	203	285	280

[a]The nucleotide numbering is in the 5′−3′ direction, and n is the affected nucleotide. The trend in other simulations is similar.

trajectories, they are not able to fully reproduce the Z-DNA backbone families. One problem appears to be associated with the α dihedral of cytosine nucleotides. Its thermal fluctuations range is almost 200°, which may indicate that the simulations are not capable of identifying any stable substate (Figure 7). Parm99 incorrectly samples values around 250°, while bsc0 moves the median closer to the correct values, but the fluctuation range is still over 200° (Table 12).

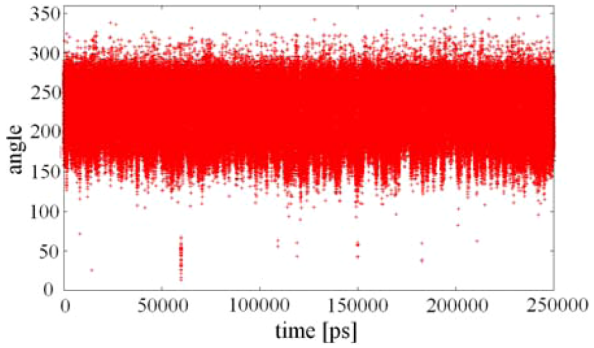

Figure 7. Development of nucleotide C17 α dihedral in net-neutral Na^+, TIP3P simulation of Z-DNA with bsc0 force field. The median value is close to the reference value; however, the fluctuation range exceeds 200°, so that the backbone apparently is unable to find a stable position.

The simulations do not reproduce the "ZI/ZII" rule. Both ZI and ZII β values of cytosine nucleotides are populated in simulations; however, the switch between β dihedral ZI and ZII values is not coupled to corresponding changes in other dihedrals. This creates a hybrid version of the two GpC conformers: β being dominantly ZII, γ and ζ being ZI, and α and ε remaining undefined (Table 12).

Among the tested force fields, it appears that bsc0 provides the best description of the Z-DNA. Even this force field does not follow correctly the ZI/ZII rule. The correct ZI or ZII ζ G(N)/β C(N+1) combinations have only 39% (TIP3P/Na^+) population while a population of 61% is seen for the wrong combination of the angles, namely β ZII combined with ζ ZI. The dynamics is reversible and the ζ–β populations oscillate on a time scale of a few nanoseconds. Another problem with bsc0 (besides the obvious α instability) is that it allows some visits from guanine γ(t) to the canonical values (Table 13). These visits are reversible on the present simulation time scales (Figure 8). This somewhat affects the median angles of α and γ in the tables. Still, since the guanines of Z-DNA in experiments are invariably in γ-trans, this dynamics is likely undesirable, though still acceptable. Compared with ff99, bsc0 slightly improves α dihedrals of cytosine nucleotides, although it is still far from correct (see above). The overall balance of the backbone description is seemingly imperfect. To confidently claim correct force field performance all the angles would have to fit the experimental family.

Table 13. Mean Population of α(+)/γ(t) in *syn*-Base Nucleotides for Z-DNA TIP3P Simulations (in % of time)

ff99	99.9
bsc0	94.6
bsc0χ_{OL3}	32.1
bsc0χ_{OL4}	53.1

Ff99 appears to rather well perform for Z-DNA. There are no γ-trans substates populated on our time scale for cytosines, while the γ-trans conformation is kept for guanines. This is

Table 12. Dihedral Angles and Pucker (in deg) of Z-DNA, Na^+-Net Neutral Simulations in TIP3P, Reference Values (the first item on each line), and Median Simulation Values (the 220–250 ns period)[a]

	cytosine nucleotides				
dihedral	ref	ff99	bsc0	bsc0χ_{OL3}	bsc0χ_{OL4}
α[b]	210/169	254	218	190	199
β	233/162	225 (8%)/164 (92%)	225 (25%)/169 (75%)	191[b]	194[b]
γ[c]	54/44[c]	44	55	59	59
δ	144	134	133	121	128
ε	264	272	274	282	279
ζ	76	69	70	76	74
χ	205	198	199	195	193
P	155	141	139	126	134
	guanine nucleotides				
dihedral	ref	ff99	bsc0	bsc0χ_{OL3}	bsc0χ_{OL4}
α	66	71	87	186	161
β	186	186	185	176	175
γ	179	182	166	80	106
δ	95	104	100	132	103
ε[b]	242/187	277	257	205	224
ζ	292/63	305 (88%)/50 (12%)	304 (86%)/50 (14%)	300[b]	305 (94%)/41 (6%)
χ	60.7	57	60	104	70
P	30–90	38	42	141	77

[a]Both ZI and ZII substates are listed where relevant. Numbers in parentheses indicate occupation time of given substate. Terminal residues are not considered. See Figure S7 (Supporting Information) for the values obtained for the individual nucleotides. Note that the simulations are mixing ZI-like and ZII-like values for different dihedrals (see the text). [b]Distinct ZI/ZII values were not stabilized in simulations. The dihedral fluctuates wildly. [c]ZII value of γ dihedral was observed for ff99 and ZI value for bsc0, bsc0χ_{OL3}, and bsc0χ_{OL4}.

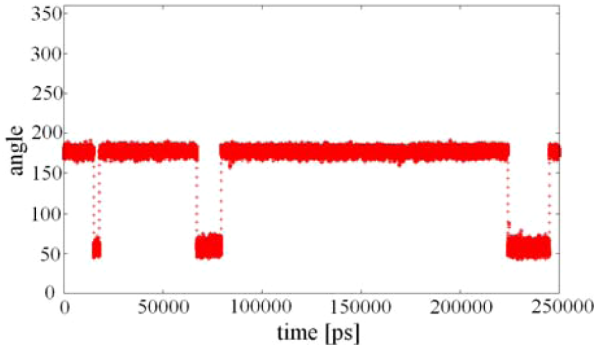

Figure 8. Development of nucleotide G8 γ dihedral in net-neutral Na^+, TIP3P simulation of Z-DNA with bsc0 force field.

consistent with experiment. However, the average α values of ~250° are very clearly outside the Z-DNA range (Table 12). Thus, both parm99 and bsc0 perform comparably for Z-DNA but are not perfect. There is no guarantee the molecule would not undergo bigger perturbation or entire degradation on a longer time scale. While the stiffness of the Z-DNA molecule keeps the overall shape intact (Supporting Information, Figure S6), the dihedral angle combinations do not correspond to those in the experiments (Table 11). Note also that ff99 is definitely not a correct DNA force field. It produces visible problems in simulations of other NA forms and disagrees with QM computations.[8] Thus, its relatively good performance for Z-DNA is incidental.

In contrast to G-DNA stems, the bsc0χ_{OL4} parametrization does not improve the performance for Z-DNA, even for the χ angle itself. Nevertheless, the helix is not visibly distorted. The RNA-specific bsc0χ_{OL3} performs poorly for Z-DNA. The lack of improvement of Z-DNA description with χ_{OL3} and χ_{OL4} modifications can be paradoxically traced to the improved *syn*-region of guanine nucleotides. Considering the potential energy surface of guanine nucleoside, ff99 and bsc0 give *syn* minimum for χ around 45° while in χ_{OL3} and χ_{OL4} it is ~60°. The later value coincides with the 61° Z-DNA reference value. However, in simulations, unfavorable changes in Z-DNA backbone (like elimination of $\alpha(+)/\gamma(t)$; see Table 13) are associated with slight increase (from ~60° to ~70°) of *syn*-base χ dihedrals. It is facilitated by the χ_{OL3} and χ_{OL4} force fields with their improved *syn* regions. It appears that the force field in general has difficulty describing the Z-DNA backbone. Then, locally improving the χ profile may result in unmasking the overall struggle. More complete refinement (perhaps α and β dihedrals) would likely be required before the simulations of Z-DNA can benefit from the improved *syn*-region. With the RNA-specific bsc0χ_{OL3} force field, χ-dihedral angles of guanine nucleotides in Z-DNA simulations increase from a reference value of ~60° to almost 110°. It is accompanied by degradation of all the other backbone angles, and the overall structure of the helix is visibly perturbed (Supporting Information , Figure S6). This is one of the reasons why the χ profile in the *syn* region has been sharpened for the DNA bsc0χ_{OL4} variant to prevent *syn* shift to the ~110° value, which is also consistent with QM computations for DNA nucleosides. This was sufficient to stabilize the overall Z-DNA topology.

The surprisingly large response of the Z-DNA to rather small modifications of the χ profile is consistent with the explanation that the problems in Z-DNA description are not due to the *syn* χ dihedral profile per se. They likely reflect a more fundamental struggle of the force field backbone description for Z-DNA, which for certain χ parameters leads to fast degradation of the molecule. To clarify this issue will require further work including extensive QM computations. Nevertheless, it is evident that Z-DNA is an important and well-defined reference structure for further refinement of the force field. There have been some occasional MD studies of Z-DNA in the literature[64] but none reporting analysis of the performance of the force field for the Z-DNA backbone. We would like to nevertheless emphasize that except of the RNA specific bsc0χ_{OL3} force field, the other force fields keep the basic Z-DNA topology stable. Interestingly, in a recent reparametrization of the CHARMM force field, the authors reported unstable Z-DNA trajectories and major unwinding in solution simulations even on a 100 ns time scale, while simulation with inclusion of the crystal lattice was satisfactory.[16] It has been suggested that the instability of solution simulations may correctly reflect the genuine instability of Z-DNA under the given solution simulation condition, which should not stabilize Z-DNA. However, the time scale of such instability might be, in our opinion, too fast.

We performed additional 200 ns long simulation of Z-DNA in high-salt conditions (1 M KCl, SPC/E with the bsc0 force field) to assess the possible influence of salt concentration on the Z-DNA dynamics. The simulation behavior was virtually identical with the equivalent minimal-salt simulations. Therefore, we suggest that the inaccurate description of Z-DNA backbone (see above) is not caused by the low ion concentration. Additionally, although the original X-ray crystal structure contained spermine molecule, its presence was earlier reported to have no effect on the ZI/ZII rule.[65] We reiterate that the problem in Z-DNA simulations is not the population of the different substates (which obviously may be sensitive to the crystal effects, spermine, and ions) but the fact that we basically dominantly sample an incorrect angle combination which is not known from the experiments.

TIP5P Simulations. As noted above, there are some differences between the TIP3P and SPC/E water models in the simulations, consistent with recent observation of dependence of RNA structural dynamics on the water model.[48] Despite that the solute force field exerts the dominant effect, its performance could be coupled with the water model. Thus, as part of our study, we also tested TIP5P water model with bsc0, bsc0χ_{OL3}, and bsc0χ_{OL4} force fields (the outdated ff99 was not considered for this test). While the basic trends are similar to those seen in equivalent TIP3P and SPC/E simulations (see above), we also noticed some differences. Namely, pucker degradation of inner-tetrads *syn*-base nucleotides in antiparallel DNA quadruplex was somewhat mitigated (Supporting Information, Tables S2 and S3). Z-DNA backbone inaccuracies observed with bsc0χ_{OL3} and bsc0χ_{OL4} force fields were also highly reduced, and bsc0χ_{OL4} was fully comparable with bsc0. Visible distortion of Z-DNA helix by bsc0χ_{OL3} was eliminated when using TIP5P (Supporting Information, Table S24), at least on our simulation time scale. While the water model seemingly performed differently in comparison with TIP3P and SPC/E, the result must be interpreted very carefully. The ion parameters are not adapted for this water model, which may affect the results. We do not know how the differences may develop on longer time scale. We also do not know how the TIP5P model would perform for other NA forms including the canonical B-DNA and A-RNA helices, since there is no experience in using TIP5P for biomolecular simulations. Such

investigations are outside the scope of the present study and will be pursued in the near future.

It should be noted that some effect of the water model on the nucleic acids simulations is indeed not ruled out. Especially the phosphates are heavily exposed to solvent, so that different water models can result in different screening of the interphosphate electrostatic repulsion and different specific hydration. Because the nucleic acids backbone torsions are highly correlated, this may induce concerted changes in balance of substates propagating along the whole sugar−phosphate backbone. Since the number of water molecules in simulations is much larger than the number of ions, the water model may easily have larger impact on simulations than the ion model and ion conditions.

Backup Simulations. The above analyses are based on detail assessment of 56 100−250 ns simulations with total length of 8.4 μs. We have subsequently carried out prolonged selected simulations (in one case up to 2 μs) so that the total amount of all simulations reached 18.0 μs. The simulations were monitored to ensure that the conclusions based on the initial set of simulations do not change. The list of prolonged simulations with some specific comments can be found in the Supporting Information (Table S27).

CONCLUSIONS

Refinement of empirical force fields for nucleic acids requires their extensive testing using as wide a range of systems as possible. However, finding unambiguous reference data is not easy. In this paper, we in detail analyze four systems that we suggest should be included in standard portfolio of molecules to test nucleic acids force fields, namely, parallel and antiparallel stranded DNA guanine quadruplex (G-DNA) stems, RNA quadruplex stem (G-RNA), and Z-DNA.

Antiparallel G-DNA is an excellent target for simulations, as it contains alternation of *syn*- and *anti*-nucleotides. In addition, we found intricate rules (confirmed by number of independent experimental structures) describing noncanonical α/γ substates of the backbone of *syn*-nucleotides in antiparallel G-DNA stem, which also appear to be useful for testing the force fields.

Parallel-stranded all-*anti* G-DNA stem is at first sight a relatively simple structure for force field description, which is confirmed also by present simulations. However, detailed scrutiny of the simulations revealed that while the backbone of parallel stranded G-DNA is described rather well, there are still modest differences between the experimental and computed values of the backbone torsions which may be improved by future force field tuning. In other words, the description of this molecule is not as perfect as assumed in the literature until now.

Although ultrahigh resolution of G-RNA stem is available, its closer scrutiny reveals that it is not useful as a benchmark, due to likely profound crystal packing effects. Nevertheless, G-RNA can still be used in testing by assuming canonical RNA backbone topology.

Z-DNA has very intricate noncanonical backbone arrangement with a specific ZI/ZII "dinucleotide" rule, where ζ angles of guanines determine β angles of subsequent (downstream) cytosines. Z-DNA is thus a tough target for simulation force fields, and indeed, none of them so far can fully reproduce the Z-DNA backbone substates, albeit globally stable simulations can be achieved.

It should be noted that force-field validation using crystallographic data, which is the essence of our work, has also its limitations. As with any other experiment, also the X-ray structures have limited accuracy, being affected by data/refinement errors and uncertainties.[24,25,66−69] Disorder may be found even in higher resolution nucleic acid structures, especially around phosphate groups, and may affect for example some high-resolution B-DNA structures as well as the ZI/ZII conformer issue. However, we would like to suggest that still the X-ray structures represent the best choice of benchmark data, i.e., for those molecules that were considered in our study we do not see any better alternative. Definitely, all the reference values given in this paper should be considered as representing the expected approximate ranges of values defining the NA backbone families rather than being some exact target values.

The work is primarily based on 8.4 μs of in detail analyzed 100−250 ns trajectories followed by 9.6 μs of additional selected backup trajectories that were monitored to verify that the results of the initial analyses are correct. Four versions of the Cornell et al. AMBER force field and three water models are tested.

We present an entirely new parmχ_{OL4} variant of the Cornell et al. force field with the χ dihedral specifically reparametrized for DNA molecules containing *syn*-nucleotides. While improvement for DNA quadruplexes is visible, we so far could not improve the description of the Z-DNA intricate backbone conformation. The parmχ_{OL4} slightly increases the helical twist of B-DNA.

ASSOCIATED CONTENT

Supporting Information

Parameter files with the χ_{OL4} parameters (standard formats), numerous graphs with dihedral development of the individual nucleotides, tables of TIP5P and excess-salt simulations, table of B-DNA performance, tables of G-RNA simulations, and brief analysis of ∼10 μs of backup simulations. This material is available free of charge via the Internet at http://pubs.acs.org.

AUTHOR INFORMATION

Corresponding Author

*E-mail: petr.jurecka@upol.cz (P.J.), sponer@ncbr.muni.cz (J.S.).

Author Contributions

#M.K. and M.Z. contributed equally to the work.

Notes

The authors declare no competing financial interest.

ACKNOWLEDGMENTS

This work was supported by the Grant Agency of the Czech Republic (grants 203/09/H046, 203/09/1476, P208/10/1742, P208/11/1822 and P305/12/G03) and "CEITEC - Central European Institute of Technology" (CZ.1.05/1.1.00/02.0068) from European Regional Development Fund. It was also supported by the Operational Program Research and Development for Innovations−European Social Fund (CZ.1.05/2.1.00/03.0058 and CZ.1.07/2.3.00/20.0017). T.E.C. was supported by NIH (grant GM-081411) and the NSF XSEDE (grant MCA01S027).

REFERENCES

(1) Ditzler, M. A.; Otyepka, M.; Sponer, J.; Walter, N. G. *Acc. Chem. Res.* **2010**, *43*, 40−47.

(2) Besseova, I.; Otyepka, M.; Reblova, K.; Sponer, J. *Phys. Chem. Chem. Phys.* **2009**, *11*, 10701−10711.

(3) Gaillard, T.; Case, D. A. *J. Chem. Theory Comput.* **2011**, *7*, 3181−3198.
(4) Šponer, J.; Cang, X.; Cheatham, T. E., III *Methods*, in press.
(5) Cornell, W. D.; Cieplak, P.; Bayly, C. I.; Gould, I. R.; Merz, K. M.; Ferguson, D. M.; Spellmeyer, D. C.; Fox, T.; Caldwell, J. W.; Kollman, P. A. *J. Am. Chem. Soc.* **1995**, *117*, 5179−5197.
(6) Cheatham, T. E., III; Cieplak, P.; Kollman, P. A. *J. Biomol. Struct. Dyn.* **1999**, *16*, 845−862.
(7) Wang, J.; Cieplak, P.; Kollman, P. A. *J. Comput. Chem.* **2000**, *21*, 1049−1074.
(8) Perez, A.; Marchan, I.; Svozil, D.; Sponer, J.; Cheatham, T. E.; Laughton, C. A.; Orozco, M. *Biophys. J.* **2007**, *92*, 3817−3829.
(9) Banas, P.; Hollas, D.; Zgarbova, M.; Jurecka, P.; Orozco, M.; Cheatham, T. E.; Sponer, J.; Otyepka, M. *J. Chem. Theory Comput.* **2010**, *6*, 3836−3849.
(10) Zgarbova, M.; Otyepka, M.; Sponer, J.; Mladek, A.; Banas, P.; Cheatham, T. E.; Jurecka, P. *J. Chem. Theory Comput.* **2011**, *7*, 2886−2902.
(11) Ode, H.; Matsuo, Y.; Neya, S.; Hoshino, T. *J. Comput. Chem.* **2008**, *29*, 2531−2542.
(12) Yildirim, I.; Stern, H. A.; Kennedy, S. D.; Tubbs, J. D.; Turner, D. H. *J. Chem. Theory Comput.* **2010**, *6*, 1520−1531.
(13) Yildirim, I.; Kennedy, S. D.; Stern, H. A.; Hart, J. M.; Kierzek, R.; Turner, D. H. *J. Chem. Theory Comput.* **2011**, *8*, 172−181.
(14) Foloppe, N.; MacKerell, A. D. *J. Comput. Chem.* **2000**, *21*, 86−104.
(15) Denning, E. J.; Priyakumar, U. D.; Nilsson, L.; Mackerell, A. D. *J. Comput. Chem.* **2011**, *32*, 1929−1943.
(16) Hart, K.; Foloppe, N.; Baker, C. M.; Denning, E. J.; Nilsson, L.; MacKerell, A. D. *J. Chem. Theory Comput.* **2012**, *8*, 348−362.
(17) Cheatham, T. E., III; Miller, J. L.; Fox, T.; Darden, T. A.; Kollman, P. A. *J. Am. Chem. Soc.* **1995**, *117*, 4193−4194.
(18) Cheatham, T. E., III; Kollman, P. A. *J. Am. Chem. Soc.* **1997**, *119*, 4805−4825.
(19) Fadrna, E.; Spackova, N.; Stefl, R.; Koca, J.; Cheatham, T. E.; Sponer, J. *Biophys. J.* **2004**, *87*, 227−242.
(20) Svozil, D.; Sponer, J. E.; Marchan, I.; Perez, A.; Cheatham, T. E., III; Forti, F.; Luque, F. J.; Orozco, M.; Sponer, J. *J. Phys. Chem. B* **2008**, *112*, 8188−8197.
(21) Mlynsky, V.; Banas, P.; Hollas, D.; Reblova, K.; Walter, N. G.; Sponer, J.; Otyepka, M. *J. Phys. Chem. B* **2010**, *114*, 6642−6652.
(22) Fadrna, E.; Spackova, N.; Sarzynska, J.; Koca, J.; Orozco, M.; Cheatham, T. E.; Kulinski, T.; Sponer, J. *J. Chem. Theory Comput.* **2009**, *5*, 2514−2530.
(23) Spackova, N.; Sponer, J. *Nucleic Acids Res.* **2006**, *34*, 697−708.
(24) Mladek, A.; Sponer, J. E.; Kulhanek, P.; Lu, X. J.; Olson, W. K.; Sponer, J. *J. Chem. Theory Comput.* **2012**, *8*, 335−347.
(25) Svozil, D.; Kalina, J.; Omelka, M.; Schneider, B. *Nucleic Acids Res.* **2008**, *36*, 3690−3706.
(26) Sponer, J.; Spackova, N. *Methods* **2007**, *43*, 278−290.
(27) Phillips, K.; Dauter, Z.; Murchie, A. I. H.; Lilley, D. M. J.; Luisi, B. *J. Mol. Biol.* **1997**, *273*, 171−182.
(28) Deng, J. P.; Xiong, Y.; Sundaralingam, M. *Proc. Natl. Acad. Sci. U. S. A.* **2001**, *98*, 13665−13670.
(29) Tereshko, V.; Wilds, C. J.; Minasov, G.; Prakash, T. P.; Maier, M. A.; Howard, A.; Wawrzak, Z.; Manoharan, M.; Egli, M. *Nucleic Acids Res.* **2001**, *29*, 1208−1215.
(30) Case, D. A.; Darden,T.; Cheatham, T. E., III; Simmerling, C. L.; Wang, J.; Duke, R. E.; Luo, R.; Crowley, M.; Walker, R., Zhang, W.; Merz, K. M.; B.Wang, Hayik, S.; Roitberg, A.; Seabra, G.; I.; Kolossváry, I.; Wong, K. F. ; Paesani, F.; Vanicek, J.; Wu, X., Brozell, S. R.; Steinbrecher, T.; Gohlke, H.; Yang, L.; Tan, C.; Mongan, J.; Hornak, V.; Cui, G.; Mathews, D. H.; Seetin, M. G.; Sagui, C.; Babin, V.; Kollman, P. A. *Amber 10*; University of California, San Francisco, 2008.
(31) Cheatham, T. E.; Cieplak, P.; Kollman, P. A. *J. Biomol. Struct. Dyn.* **1999**, *16*, 845−862.
(32) Krishnan, R.; Binkley, J. S.; Seeger, R.; Pople, J. A. *J. Chem. Phys.* **1980**, *72*, 650−654.
(33) Clark, T.; Chandrasekhar, J.; Spitznagel, G. W.; Schleyer, P. V. *J. Comput. Chem.* **1983**, *4*, 294−301.
(34) Gill, P. M. W.; Johnson, B. G.; Pople, J. A. *J. Chem. Phys.* **1992**, *96*, 7178−7179.
(35) Frisch, M. J.; Pople, J. A.; Binkley, J. S. *J. Chem. Phys.* **1984**, *80*, 3265−3269.
(36) Klamt, A.; Schuurmann, G. *J. Chem. Soc., Perkin Trans. 2* **1993**, 799−805.
(37) Ahlrichs, R.; Bar, M.; Haser, M.; Horn, H.; Kolmel, C. *Chem. Phys. Lett.* **1989**, *162*, 165−169.
(38) Halkier, A.; Helgaker, T.; Jorgensen, P.; Klopper, W.; Koch, H.; Olsen, J.; Wilson, A. K. *Chem. Phys. Lett.* **1998**, *286*, 243−252.
(39) Halkier, A.; Helgaker, T.; Jorgensen, P.; Klopper, W.; Olsen, J. *Chem. Phys. Lett.* **1999**, *302*, 437−446.
(40) Frisch, M. J.; Trucks, G. W.; Schlegel, H. B.; Scuseria, G. E.; Robb, M. A.; Cheeseman, J. R.; Montgomery, J. A.; Vreven, T.; Kudin, K. N.; Burant, J. C.; Millam, J. M.; Iyengar, S. S.; Tomasi, J.; Barone, V.; Mennucci, B.; Cossi, M.; Scalmani, G.; Rega, N.; Petersson, G. A.; Nakatsuji, H.; Hada, M.; Ehara, M.; Toyota, K.; Fukuda, R.; Hasegawa, J.; Ishida, M.; Nakajima, T.; Honda, Y.; Kitao, O.; Nakai, H.; Klene, M.; Li, X.; Knox, J. E.; Hratchian, H. P.; Cross, J. B.; Bakken, V.; Adamo, C.; Jaramillo, J.; Gomperts, R.; Stratmann, R. E.; Yazyev, O.; Austin, A. J.; Cammi, R.; Pomelli, C.; Ochterski, J. W.; Ayala, P. Y.; Morokuma, K.; Voth, G. A.; Salvador, P.; Dannenberg, J. J.; Zakrzewski, V. G.; Dapprich, S.; Daniels, A. D.; Strain, M. C.; Farkas, O.; Malick, D. K.; Rabuck, A. D.; Raghavachari, K.; Foresman, J. B.; Ortiz, J. V.; Cui, Q.; Baboul, A. G.; Clifford, S.; Cioslowski, J.; Stefanov, B. B.; Liu, G.; Liashenko, A.; Piskorz, P.; Komaromi, I.; Martin, R. L.; Fox, D. J.; Keith, T.; Laham, A.; Peng, C. Y.; Nanayakkara, A.; Challacombe, M.; Gill, P. M. W.; Johnson, B.; Chen, W.; Wong, M. W.; Gonzalez, C.; Pople, J. A. *Gaussian 03*, Revision C.02; Gaussian, Inc.: Wallingford, CT, 2004.
(41) Jorgensen, W. L.; Chandrasekhar, J.; Madura, J. D.; Impey, R. W.; Klein, M. L. *J. Chem. Phys.* **1983**, *79*, 926−935.
(42) Jorgensen, W. L. *J. Am. Chem. Soc.* **1981**, *103*, 335−340.
(43) Berendsen, H. J. C.; Grigera, J. R.; Straatsma, T. P. *J. Phys. Chem.* **1987**, *91*, 6269−6271.
(44) Mahoney, M. W.; Jorgensen, W. L. *J. Chem. Phys.* **2000**, *112*, 8910−8922.
(45) Aqvist, J. *J. Phys. Chem.* **1990**, *94*, 8021−8024.
(46) Dang, L. X.; Kollman, P. A. *J. Phys. Chem.* **1995**, *99*, 55−58.
(47) Smith, D. E.; Dang, L. X. *J. Chem. Phys.* **1994**, *100*, 3757−3766.
(48) Sklenovsky, P.; Florova, P.; Banas, P.; Reblova, K.; Lankas, F.; Otyepka, M.; Sponer, J. *J. Chem. Theory Comput.* **2011**, *7*, 2963−2980.
(49) Darden, T.; York, D.; Pedersen, L. *J. Chem. Phys.* **1993**, *98*, 10089−10092.
(50) Essmann, U.; Perera, L.; Berkowitz, M. L.; Darden, T.; Lee, H.; Pedersen, L. G. *J. Chem. Phys.* **1995**, *103*, 8577−8593.
(51) Berendsen, H. J. C.; Postma, J. P. M.; Vangunsteren, W. F.; Dinola, A.; Haak, J. R. *J. Chem. Phys.* **1984**, *81*, 3684−3690.
(52) Reblova, K.; Fadrna, E.; Sarzynska, J.; Kulinski, T.; Kulhanek, P.; Ennifar, E.; Koca, J.; Sponer, J. *Biophys. J.* **2007**, *93*, 3932−3949.
(53) Besseova, I.; Otyepka, M.; Reblova, K.; Sponer, J. *Phys. Chem. Chem. Phys.* **2009**, *11*, 10701−10711.
(54) Humphrey, W.; Dalke, A.; Schulten, K. *J. Mol. Graph.* **1996**, *14*, 33−&.
(55) Altona, C.; Sundaralingam, M. *J. Am. Chem. Soc.* **1972**, *94*, 8205−&.
(56) Haider, S.; Parkinson, G. N.; Neidle, S. *J. Mol. Biol.* **2002**, *320*, 189−200.
(57) Horvath, M. P.; Schultz, S. C. *J. Mol. Biol.* **2001**, *310*, 367−377.
(58) Hazel, P.; Parkinson, G. N.; Neidle, S. *J. Am. Chem. Soc.* **2006**, *128*, 5480−5487.
(59) Campbell, N. H.; Smith, D. L.; Reszka, A. P.; Neidle, S.; O'Hagan, D. *Org. Biomol. Chem.* **2011**, *9*, 1328−1331.
(60) Gill, M. L.; Strobel, S. A.; Loria, J. P. *Nucleic Acids Res.* **2006**, *34*, 4506−4514.
(61) Brzezinski, K.; Brzuszkiewicz, A.; Dauter, M.; Kubicki, M.; Jaskolski, M.; Dauter, Z. *Nucleic Acids Res.* **2011**, *39*, 6238−6248.

(62) Dauter, Z.; Adamiak, D. A. *Acta Crystallogr., Sect. D: Biol. Crystallogr.* **2001**, *57*, 990−995.
(63) Gessner, R. V.; Frederick, C. A.; Quigley, G. J.; Rich, A.; Wang, A. H. J. *J. Biol. Chem.* **1989**, *264*, 7921−7935.
(64) Lee, J.; Kim, Y. G.; Kim, K. K.; Seok, C. *J. Phys. Chem. B* **2010**, *114*, 9872−9881.
(65) Wang, A. H. J.; Quigley, G. J.; Kolpak, F. J.; Vandermarel, G.; Vanboom, J. H.; Rich, A. *Science* **1981**, *211*, 171−176.
(66) Dickerson, R. E.; Grzeskowiak, K.; Grzeskowiak, M.; Kopka, M. L.; Larsen, T.; Lipanov, A.; Prive, G. G.; Quintana, J.; Schultze, P.; Yanagi, K.; Yuan, H.; Yoon, H. C. *Nucleosides, Nucleotides Nucleic Acids* **1991**, *10*, 3−24.
(67) Sponer, J.; Kypr, J. *J. Biomol. Struct. Dyn.* **1993**, *11*, 277−292.
(68) Dickerson, R. E.; Goodsell, D. S.; Neidle, S. *Proc. Natl. Acad. Sci. U. S. A.* **1994**, *91*, 3579−3583.
(69) Kielkopf, C. L.; Ding, S.; Kuhn, P.; Rees, D. C. *J. Mol. Biol.* **2000**, *296*, 787−801.